Thermocapillary effects in two-phase medium and applications to metal-silicate separation

Yanick Ricard [a],[*], Stéphane Labrosse [a], Hidenori Terasaki [b], David Bercovici [c]

[a] *Université de Lyon, ENSL, UCBL, Laboratoire LGLTPE, 15 parvis René Descartes, BP7000, 69342 Lyon, Cedex 07, France*
[b] *Okayama University, Department of Earth Sciences, Tsushimanaka 3-1-1, Kita-ku, Okayama 700-8530, Japan*
[c] *Yale University, Department of Earth & Planetary Sciences, P.O. Box 208109, New Haven, CT 06520-8109, USA*

ABSTRACT

The separation of a liquid phase from a solid but deformable matrix made of mineral grains is controlled at small scale by surface tension. The role of interfacial surface tension is twofold as it explains how a small volume of liquid phase can infiltrate the grain boundaries, be distributed and absorbed in the matrix, but after complete wetting of the grains, surface tension favors the self-separation of the liquid and solid phases. Another consequence of surface tension is the existence of Marangoni forces, which are related to the gradients of surface tension that are are usually due to temperature variations. In this paper, using a continuous multi-phase formalism we clarify the role of these different effects and quantify their importances at the scale of laboratory experiments and in planets. We show that Marangoni forces can control the liquid metal-solid silicate phase separation in laboratory experiments. The Marangoni force might help to maintain the presence of metal at the surface of asteroids and planetesimals that have undergone significant melting.

1. Introduction

Storage and migration of a liquid phase inside a solid but deformable matrix occurs in various situations in terrestrial bodies, whether it be in their near surface, or in their deep interiors such at the Earth's core-mantle boundary (CMB) or the core-inner core boundary. The equilibrium geometry of a given fraction of fluid phase dispersed into a matrix made of crystal grains is controlled by the ratio of the surface energy between grains to that between a solid grain and the liquid (see Rudge, 2018, for a thorough description of the phase diagram of the possible interface topologies). At small porosity, i.e., at small fluid volume fraction, the capillary forces control whether the fluid is confined into isolated bubbles or forms an interconnected pattern of tubules at grain triple junctions (von Bargen and Waff, 1986; Hier-Majumder and Kohlstedt, 2006). When a network of fluid tubules is established, a Darcy flow of the fluid phase is possible and controlled by the properties of the two phases including the strength of the matrix. During this stage, the matrix can absorb the fluid if placed in contact with it and the capillary forces tend to homogenize the volume fraction of fluid within the matrix. At larger fluid content, however, when the grains of the matrix are totally wetted, the capillary forces give rise to self separation of the solid and liquid phases (Hier-Majumder et al., 2006). For the Earth, gravity forces are much larger than capillary forces and it is only at a microscopic scale that the influences of the latter are important.

In planetesimals, which are the building blocks of planets, metal silicate separation seems to have occurred very early. From the observation of meteorites, melting occurred when their parent bodies that were in the range of 50–200 km radius (Rasmussen et al., 2001). The thermal histories of these small bodies are strong functions of their accretion mechanisms. Some authors (e.g., Yoshino et al., 2003; Walter and Tronnes, 2004) suggest that radiogenic heating from unstable isotopes such as ^{26}Al or ^{60}Fe, was intense enough to melt planetesimals of only a few 10 km radius. More refined simulations suggest that planetesimals needed to be slightly larger ($\approx$100 km) to reach melting temperatures (Šrámek et al., 2012; Ricard et al., 2017). However, planetesimals were possibly significantly molten when their radii were less than two orders of magnitude smaller than that of the Earth. For such small bodies, the gravity is two–three orders of magnitude smaller than that of the Earth and the relative importance of capillary forces is commensurately increased.

The behavior of metallic melt in contact with silicates has been studied experimentally by various researchers (Knittle and Jeanloz, 1991; Goarant et al., 1992; Terasaki et al., 2008; Yoshino, 2019) and interpreted considering a uniform surface tension between phases. However, at the very small scale of high pressure laboratory experiments, the inhomogeneity of the temperature can create capillary forces related to the gradient of surface tension. These forces, called Marangoni forces (Marangoni, 1871), are related to surface tension gradients rather

than to the effects of interface curvature; the Marangoni effect affected the experiments in Henri Bénard's seminal study of thermal convection (Bénard, 1900, 1901). Their omission in the framework of thermal convection developed by Lord Rayleigh led to discrepancies between observations and theory for many decades (Block, 1956; Bercovici, 2007). These forces are not necessarily dominant in geological settings and are not the forces that are typically associated with homogeneous surface tension (such as wetting, infiltration, or self-separation) and discussed e.g., in the framework of metal-silicate interaction at the CMB (Poirier and Le Mouël, 1992). Here we explore and clarify the role of the Marangoni effect in two-phase theory and in experiments on metal melts in silicates and discuss its importance particularly in small partially molten planetesimals.

2. Thermocapillary effects

The existence of thermocapillary forces is related to the classic expression of stress balance across interfaces. If we denote by [[ ]] the jump of a quantity across an interface Σ perpendicular to its unit vector **n**, the stress tensor **T** discontinuity is

$$\left[\left[\underline{\mathbf{T}}.\mathbf{n}\right]\right] = \sigma\kappa\mathbf{n} - \nabla_t\sigma \tag{1}$$

where σ is the surface tension, $\kappa = \nabla \cdot \mathbf{n}$ is the sum of the principal curvatures of Σ (κ is thus 2 times the inverse radius for a spherical bubble or the inverse radius for a cylindrical tubule), and ∇_t is the gradient, tangent to Σ. The interface induces a discontinuity of the normal stress, $\sigma\kappa\mathbf{n}$ (which in steady-state situation is Laplace's condition: there exists an overpressure equal to $2\sigma/R$ between the concave and convex sides of a spherical bubble of radius R) as well as a discontinuity in the shear stress equal to $\nabla_t\sigma$ when σ, for example, is a function of a non uniform temperature. The shear stress discontinuity induces the Marangoni effect.

2.1. Thermocapillary force on a single bubble or drop

In the situations we seek to model - a fluid phase percolating through a permeable matrix or a suspension of one phase moving through the other, in the presence of thermal gradient - we do not want to describe precisely the interfaces between the phases which are highly convolved at the fluid pore and matrix grain scale. We use a continuous approach akin to what has been proposed by McKenzie (1984) or Scott and Stevenson (1984) based on the work of Drew and Segel (1971). This formalism has been generalized to account for the presence of surface tension (Bercovici et al., 2001; Bercovici and Ricard, 2003). However, when the effects of surface tension have been considered (Ricard et al., 2001; Hier-Majumder et al., 2006), surface tension was assumed uniform. Here, we extend this formalism by including the spatial variations of interfacial tension. We shall first check that the behavior of the two-phase equations is in qualitative agreement with well known physical experiments done on simpler systems.

Gas bubbles in a liquid can be held stationary or even be driven downward by imposing a negative temperature gradient opposite gravity (Young et al., 1959; Harper et al., 1967; Hardy, 1979). Consider a bubble of fluid with density, viscosity and thermal conductivity ρ_i, μ_i and k_i, moving into another fluid of properties ρ_o, μ_o and k_o (using indices referring to "in" and "out"). There is a surface tension σ on the interface between the phases, and the fluids are subjected to a vertical thermal gradient. Young et al. (1959) demonstrate that the vertical velocity of the bubble is

$$v_i = \frac{2}{3}\frac{1}{2\mu_o + 3\mu_i}\left[\Delta\rho gr^2\frac{\mu_o + \mu_i}{\mu_o} - \frac{3}{2 + k_i/k_o}r\frac{d\sigma}{dz}\right] \tag{2}$$

where $\Delta\rho = \rho_o - \rho_i > 0$, gravity is $\mathbf{g} = -g\mathbf{z}$, and the unit vector **z** points upward. The surface tension derivative $d\sigma/dT$ is generally negative and

a negative thermal gradient dT/dz can therefore oppose gravity. This expression can be derived following the Hadamard-Rybczynski demonstration (e.g., Batchelor, 2000) in matching the singular solution of the Stokes equation taking into account the discontinuity of shear stress at the interface using (1).

We assume a uniform thermal conductivity, $k_i = k_o$, and when $\mu_i = 0$, (2) leads to

$$v_i = \frac{1}{3\mu_o}\left[\Delta\rho gr^2 - r\frac{d\sigma}{dz}\right] \tag{3}$$

which is the Hadamard-Rybczynski relation for an inviscid bubble with a Marangoni surface tension term. The laboratory experiments of Young et al. (1959) have confirmed that bubbles can be held still in a liquid when a negative temperature gradient verifying the condition $\Delta\rho gr = \frac{d\sigma}{dT}\frac{dT}{dz}$ is imposed according to (3). In contrast when μ_i is infinite, (2) yields

$$v_i = \frac{2}{9\mu_o}\Delta\rho gr^2 \tag{4}$$

which is the Stokes relation for a rigid sphere, but in this case surface tension plays no role.

That a low viscosity sphere should travel (under gravity alone) 50% faster that solid spheres (i.e., a factor $1/3$ in (3) and $2/9$ in (4)) is not observed experimentally if bubbles are too small. A transition of the rising velocity of an inviscid bubble, from Stokes drag to Hadamard-Rybczynski drag, is experimentally observed with bubbles of increasing radii (Haberman and Morton, 1953). This is related to another and less expected consequence of the Marangoni effect. Due to the motion of the low viscosity bubble interface, convection causes contaminants to accumulate on the downstream side of the bubble (e.g., Clift et al., 1978). This creates a surface tension gradient and an effective shear stress acting in a direction opposite to the flow. This Marangoni effect related to chemical rather than thermal effects rigidifies the interfaces of small inviscid bubbles and bring their velocities close to that of rigid spheres. The effect is pronounced for small bubbles since according to (3), the Marangoni force becomes larger relative to the buoyancy force as the bubble size decreases. In this paper, we assume that the surface tension is only a function of temperature and this effect is not considered.

2.2. Thermocapillary force in continuous two-phase models

We next explore whether a continuous two-phase formalism, can account for a light phase being driven downward against its own buoyancy by imposing a negative temperature gradient in a mixture of bubbles and liquid. This formalism does not account for inertia (zero Reynolds number approximation) and assume that the two phases are incompressible, which is consistent with the assumptions of Stokes flow leading to the eq. (2) (see Fig. 1). In these equations we also assume that the temperature is in equilibrium between phases and smooth across bubbles and all the mixture, which corresponds to the case of homogeneous thermal conductivities in which $k_o = k_i$ in (2).

Using the formalism of Bercovici et al. (2001) and Bercovici and Ricard (2003), the momentum equation of the ambient phase (subscript o) writes

$$-(1-\phi)(\nabla P_o + \rho_o g\mathbf{z}) + \nabla.\left[(1-\phi)\underline{\tau}_o\right] - c\Delta\mathbf{v} + (1-\omega)[\Delta P\nabla\phi + \nabla\chi]$$
$$= 0. \tag{5}$$

This phase contains a minor phase (subscript i) with a volume fraction ϕ. The momentum equation of the minor phase is

$$-\phi(\nabla P_i + \rho_i g\mathbf{z}) + c\Delta\mathbf{v} + \omega[\Delta P\nabla\phi + \nabla\chi] = 0. \tag{6}$$

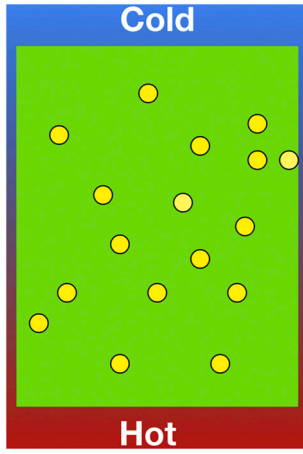In these equations, $\Delta P = P_o - P_i$ and $\Delta\mathbf{v} = \mathbf{v}_o - \mathbf{v}_i$ are the differences

Fig. 1. The major phase o is in green and the phase i in yellow. The phase i is composed of individual bubbles or drops that can be less or more viscous than the phase o. The difference of density $\Delta\rho = \rho_o - \rho_i$ between the phases is assumed positive (e.g., buoyant bubbles). In the model, the two phases are incompressible. The top temperature is lower than the bottom temperature. (For interpretation of the references to colour in this figure legend, the reader is referred to the web version of this article.)

of pressure and velocity between the two phases. A viscous stress $\underline{\tau}_o$ is present in the momentum equation of the ambient phase but neglected in the momentum equation of the minor phase. The quantity ω is between 0 and 1 and characterizes how much each phase carries the surface tension. The coefficient c accounts for the viscous drag between phases. It can represent Darcy-type flow of the minor phase percolating through the ambient phase (e.g., McKenzie, 1984; Bercovici et al., 2001) or Stokes-type flow of a suspension of solid particles in a liquid or gas, or bubbles of fluids in a viscous surrounding (e.g., Bercovici and Michaut, 2010; Michaut et al., 2013). According to Hier-Majumder et al. (2006), the surface energy per unit volume $\chi = \sigma_e\alpha$ is related to an effective surface tension σ_e which here is assumed to be a function of temperature only (the averaging of the continuous two-phase formalism causes the effective quantity to be of the same order but slightly less than the true surface tension σ, see Bercovici et al. (2001)) and the area of interfacial surface per unit volume α (in m^{-1} as it represents a quantity of interfacial surface in m^2 per unit volume of mixture in m^{-3}).

By combining the eqs. (5) and (6), an action-reaction force balance can be obtained,

$$-\phi(1-\phi)\nabla\Delta P + \phi\nabla.\left[(1-\phi)\underline{\tau}_o\right] - c\Delta\mathbf{v} - \phi(1-\phi)\Delta\rho g\mathbf{z} + (\phi$$
$$-\omega)[\Delta P\nabla\phi + \nabla\chi]$$
$$= 0, \tag{7}$$

and we show in Bercovici and Ricard (2003) that the pressure difference amounts to

$$\Delta P = -\sigma_e\frac{\partial\alpha}{\partial\phi} - \frac{4\mu_o}{3}\frac{1}{\phi(1-\phi)}[(1-\omega)(1-\phi)\nabla.\mathbf{v}_o - \omega\phi\nabla.\mathbf{v}_i] \tag{8}$$

In a static equilibrium, when $\mathbf{v}_o$ and $\mathbf{v}_i$ are zero, (8) becomes similar to the usual Laplace condition balancing the pressure jump agains surface tension times curvature. For example, in the case where there is a single stationary bubble of radius r in a volume V_0, $\alpha = 4\pi r^2/V_0$, $\phi = (4/3)\pi r^3/V_0$, and one recovers the Laplace condition $\Delta P = -2\sigma_e/r$. A difference from this equilibrium condition implies compaction or dilation and thus a change in the volume fraction of phases.

The momentum equations, (5) and (6), and the action-reaction balance (7) are supplemented by the conservation of mass that yields two alternative equations

$$\frac{\partial\phi}{\partial t} = \nabla.((1-\phi)\mathbf{v}_o) = -\nabla.(\phi\mathbf{v}_i), \tag{9}$$

from which the continuity of the average velocity is immediately deduced

$$\nabla.((1-\phi)\mathbf{v}_o + \phi\mathbf{v}_i) = 0. \tag{10}$$

In a one dimensional vertical system, in which $\mathbf{v}_i = v_i\mathbf{z}$ and $\mathbf{v}_o = v_o\mathbf{z}$, and assuming that the medium is confined between two impermeable horizontal surfaces, the continuity eq. (10) leads to

$$v_i = -\frac{1-\phi}{\phi}v_o \tag{11}$$

in which case (8) gives the jump condition

$$\Delta P = -\sigma_e\frac{\partial\alpha}{\partial\phi} - \frac{4\mu_o}{3\phi}\left[v_o' - \frac{\omega\phi'}{\phi(1-\phi)}v_o\right] \tag{12}$$

where the prime implies differentiation in z. With these relations, the action-reaction (7) becomes

$$\frac{4\mu_o}{3c}\left[\phi^2\left(\frac{1-\phi^2}{\phi}v_o'\right)' - v_o\omega\left(\phi'', -\frac{2-2\phi-\omega}{\phi(1-\phi)}\phi'^2\right) - v_o\omega'\phi'\right] - v_o = F \tag{13}$$

where

$$F = \frac{\phi^2}{c}\left[(1-\phi)\Delta\rho g - (1-\phi)\frac{d}{dz}\sigma_e\frac{\partial\alpha}{\partial\phi} - \frac{\phi-\omega}{\phi}\left(\frac{d\sigma_e\alpha}{dz} - \sigma_e\frac{\partial\alpha}{\partial\phi}\frac{d\phi}{dz}\right)\right] \tag{14}$$

Given a sufficiently large domain in z, then far from the top and bottom boundaries where compaction occurs, the velocity gradients are small, and the velocity of the major phase is given by the balance $-V_o = F$, which gives the characteristic velocity V_i of the minor phase.

$$V_i = -\frac{1-\phi}{\phi}V_o = \frac{1-\phi}{\phi}F. \tag{15}$$

The phase i will therefore rise or sink according to the sign of F. The full velocity v_i is the solution to the differential eq. (13) with the continuity eq. (11), but its amplitude is of order V_i in the middle of the domain.

2.3. Stokes motion of the minor phase

The two-phase formalism is general enough to handle motions of bubbles and drops (Stokes flow) and the motion of a fluid inside a porous matrix (Darcy flow) (e.g., Michaut et al., 2013). We first assume that the minor phase is made of a collection of bubbles or drops and then consider the viscous interaction between phases.

2.3.1. The interaction term

To develop an expression for the viscous drag coefficient c, one can proceed as follows. An isolated sphere of radius r moved by buoyancy in a fluid of average density $\phi\rho_i + (1-\phi)\rho_o$ and neglecting surface tension, rises according to the Hadamard-Rybczynski equation (e.g. Batchelor, 1972)

$$2\pi\mu_o r\frac{2\mu_o + 3\mu_i}{\mu_o + \mu_i}\Delta\mathbf{v} = \frac{4\pi}{3}r^3(\rho_i - \bar{\rho})g\mathbf{z} = -\frac{4\pi}{3}r^3(1-\phi)\Delta\rho g\mathbf{z} \tag{16}$$

which multiplied by a bubble density $\mathcal{N}$ (number of bubbles per unit volume, so that $(4/3)\pi r^3\mathcal{N} = \phi$) results in

$$\phi(1-\phi)\Delta\rho g\mathbf{z} + \frac{3\mu_o}{2r^2}\frac{2\mu_o + 3\mu_i}{\mu_o + \mu_i}\phi\Delta\mathbf{v} = 0 \tag{17}$$

assuming that the Hadamard-Rybczynski equation still holds for an ensemble of bubbles (i.e., the suspension of bubbles is dilute).

Comparing (17) with (7) suggests that

$$c = \frac{3\mu_o}{2r^2} \frac{2\mu_o + 3\mu_i}{\mu_o + \mu_i} \phi. \tag{18}$$

With this choice of the drag coefficient c, the velocity of the minor phase is

$$v_i = -(1-\phi)\Delta v = \frac{2}{3\mu_o}(1-\phi)^2 \frac{\mu_o + \mu_i}{2\mu_o + 3\mu_i} \Delta\rho g r^2. \tag{19}$$

However, this does not account for the interactions between bubbles that reduce their velocities with respect to the Stokes velocity of an isolated bubble. This hampering term has been discussed theoretically, numerically, and experimentally (Batchelor, 1972; Richardson and Zaki, 1954; Faroughi and Huber, 2015) and the velocity reduction is larger than that predicted by the $(1-\phi)^2$ term of (19). Richardson and Zaki (1954) proposed $(1-\phi)^n$ with $n \approx 4.5$. An interaction term such as

$$c = \frac{3\mu_o}{2r^2} \frac{2\mu_o + 3\mu_i}{\mu_o + \mu_i} \frac{\phi}{(1-\phi)^p} \tag{20}$$

with $p \approx 2.5$ might, therefore, be more appropriate.

2.3.2. The surface energy term for bubbles and drops

The term $\chi = \sigma_e \alpha$ is related to the energy per unit area of the surfaces, σ_e, times the quantity of surface per unit volume α; their product χ thus represents the interfacial energy per unit volume. For a mixture full of bubbles or drops of radius r with a number density $\mathcal{N}$ (number of bubbles/drops per unit volume), $\alpha = 4\pi r^2 \mathcal{N}$ and $\phi = (4/3)\pi r^3 \mathcal{N}$ and therefore

$$\alpha = 3\frac{\phi}{r}, \tag{21}$$

which indicates that α and ϕ are not uniquely related as their ratio depends on r. Furthermore the bubble radii may not all be the same. In general, in this two-phase formalism, the interface area density must be described as $\alpha(\phi,A)$, a function of the fluid volume fraction and of an inverse size $\mathscr{A}$ characterizing the topology of the interfaces (referred to as fineness in Bercovici and Ricard (2005)). Another equation could then be introduced to describe the evolution of $\mathscr{A}$ with ϕ, with pressure (if the minor phase were compressible) or with time (if bubbles can merge). This is indeed proposed and used in various papers (Bercovici and Ricard, 2005; Ricard and Bercovici, 2009; Bercovici and Ricard, 2012, 2014) dealing with evolution of the silicate grains in the Earth mantle.

2.3.3. Examples of emulsion/foam flows

In computing the pressure jump between phases (8), one has to decide whether ϕ and r (or $\mathscr{A}$) are independent variables or not. Each choice of a relation between r and ϕ must correspond to the specific physical situation to be described. For example, one can consider a situation where the bubble sizes are fixed and their volume fraction depends only on the number density of bubbles. In this case, α is a function of the single variable ϕ and the steady state pressure jump between the two phases is, according to (8),

$$\Delta P = -3\frac{\sigma_e}{r}. \tag{22}$$

Another example would be the case where the number density $\mathcal{N}$ and ϕ are independent variables and where the changes in the volume fraction of bubbles are due to variations in bubble radius, which thus implicitly becomes a function of ϕ. In this case $r = (3\phi/(4\pi\mathcal{N}))^{1/3}$ and $\alpha = 3\phi(3\phi/(4\pi\mathcal{N}))^{-1/3}$. The interface density, α is then only a function of ϕ, and the steady state pressure jump is

$$\Delta P = -2\frac{\sigma_e}{r}. \tag{23}$$

These two expressions are the equivalent in two-phase formalism of

the usual Laplace condition. Other expressions could have been obtained if we had built a more complex micro-mechanical model relating the fineness of the minor phase to its volume fraction, to time, or to other variables. The averaging procedure that yields the two-phase equations is not expected to exactly capture the complete knowledge of the phase interface morphology.

Here we simply consider that bubble radii are fixed and use (22). This assumption of an ensemble of bubbles with fixed radii seems appropriate for comparing with the single bubble of fixed radius studied by Young et al. (1959). The case where the bubble number density and the porosity are independent variables is discussed in Appendix A.

The various derivatives of (13) when $\alpha = 3\phi/r$ and r is independent of ϕ can be easily expressed as

$$\frac{d}{dz}\sigma_e\frac{\partial\alpha}{\partial\phi} = \frac{3}{r}\frac{d\sigma_e}{dz}$$
$$\frac{d\sigma_e\alpha}{dz} - \sigma_e\frac{\partial\alpha}{\partial\phi}\frac{d\phi}{dz} = 3\frac{\phi}{r}\frac{d\sigma_e}{dz} \tag{24}$$

which yields a characteristic velocity for the bubble V_i (see (15))

$$V_i = \frac{2}{3\mu_o}(1-\phi)^{p+1}\frac{\mu_o + \mu_i}{2\mu_o + 3\mu_i}\left[(1-\phi)\Delta\rho g r^2 - 3(1-\omega)r\frac{d\sigma_e}{dz}\right] \tag{25}$$

This characteristic velocity corresponds to the minor phase velocity far from the top and bottom boundary layers of a domain vertically bounded. In the expression (25), one recognizes the gravity force $((1-\phi)\Delta\rho g$ is the effective buoyancy of a bubble) and the Marangoni force due to the temperature variation of the surface tension.

In Bercovici and Ricard (2003) we discussed the value of the partitioning term ω. We showed that $\omega \to 0$ when the viscosity of the minor phase becomes negligible compared to that of the ambient phase, $\mu_i \ll \mu_o$, and $\omega \to 1$ in the opposite situation, $\mu_o \ll \mu_i$, in such a way that the surface tension force is carried by the most competent of the two fluids. In agreement with Young et al. (1959), the fact that $\omega \to 1$ when $\mu_o \ll \mu_i$ confirms that the Marangoni force has no effect when the minor phase has a large viscosity (or is formed of solid drops, see (25)). The expression that we obtain is therefore perfectly compatible, at small volume fraction ϕ, with either (3), when $\omega = 0$, or (4) when $\omega = 1$, if we choose $\sigma_e = \sigma/3$. Furthermore, if one wishes to exactly match (2) with (25) one would require

$$\omega = \frac{\mu_i}{\mu_o + \mu_i}, \tag{26}$$

in which case, we will get

$$V_i = \frac{2}{3}\frac{(1-\phi)^{p+1}}{2\mu_o + 3\mu_i}\left[(1-\phi)\frac{\mu_o + \mu_i}{\mu_o}\Delta\rho g r^2 - 3r\frac{d\sigma_e}{dz}\right] \tag{27}$$

Notice than in Bercovici and Ricard (2003) we suggested that ω might have the form $\mu_i\phi/(\mu_o(1-\phi) + \mu_i\phi)$ although the dependence on ϕ is not required. In any case for all the applications we have considered in previous papers either the viscosity ratio between phases was large enough that we used $\omega = 0$ (Ricard et al., 2001; Hier-Majumder et al., 2006), or the viscosities were nearly identical (e.g., in Bercovici and Ricard, 2005; Ricard and Bercovici, 2009; Bercovici and Ricard, 2012, 2014) in which case the phases had similar velocities and the choice of ω made no difference.

The velocity of the ambient phase is the solution to (13), which assuming $\mu_o \gg \mu_i$, $\omega = 0$, and r is uniform, can be recast as

$$\delta^2\phi(1-\phi)^p\frac{d}{d\tilde{z}}\left(\frac{1-\phi^2}{\phi}\frac{d\tilde{v}_o}{d\tilde{z}}\right) - \tilde{v}_o = F$$
$$F = \phi(1-\phi)^p\left[1-\phi-\frac{d\tilde{\sigma}}{d\tilde{z}}\right] \tag{28}$$

where the quantities with a tilde are now without dimensions. The

surface tension σ_e is divided by its value in the middle of the domain σ_0, the height z by the compaction length $l_c = 3\sigma_0/(\Delta\rho g r)$ (the bubbles are assumed less dense than the liquid such that $\Delta\rho > 0$), the velocity v_o by the Stokes velocity $v_s = \Delta\rho g r^2/(3\mu_o)$ and the normalized compaction length is $4\mu_o/(3cl_c^2)$ (notice that here, in the case where the coefficient c accounts for viscous drag occurring in a Stokes-type flow of bubbles, $\delta = 2r/(3l_c)$ according to (18)). The exact minor phase velocity can then be deduced from mass conservation (11).

To perform a numerical simulation, we choose the parameters of a laboratory experiment (Young et al., 1959), corresponding to a dimensionless compaction length in (28) $\delta = 1.8 \times 10^{-3}$ (see caption of Fig. 2). We choose $d\tilde{\sigma}/d\tilde{z} = 0.9$, corresponding to a situation where the gravity is larger than the Marangoni forces and where a dilute suspension of bubbles rises. Eq. (28) with $p = 0$, is solved numerically in finite differences using a tridiagonal solver with the boundary conditions $\tilde{v}_o = 0$ on the top and bottom (Fig. 2). The transport eq. (9), is solved using an explicit upwind method. The initial bubble volume fraction is 0.05. The bubbles start accumulating in the upper part of the domain where their volume fraction ϕ increases (panel a). When their volume fraction becomes larger than 10%, the Marangoni force cancels their collective buoyancy. Then the competition between gravity and Marangoni force, leads to compaction oscillations that are slowly decreasing in amplitude while the bottom half of the domain becomes devoid of bubbles (Fig. 2, b, c, d). Compaction oscillations are commonly found in two-phase equations, when the motion of the minor phase is impeded by an obstacle (Spiegelman, 1993; Rabinowicz et al., 2002).

2.4. Darcy motion of the minor phase

The two-phase formalism is general enough that it can be used for a Darcy type flow (see Fig. 3), where the liquid percolates through the matrix. Since the continuous two-phase approach captures the behavior of non-uniform surface tension, we can apply this formalism to
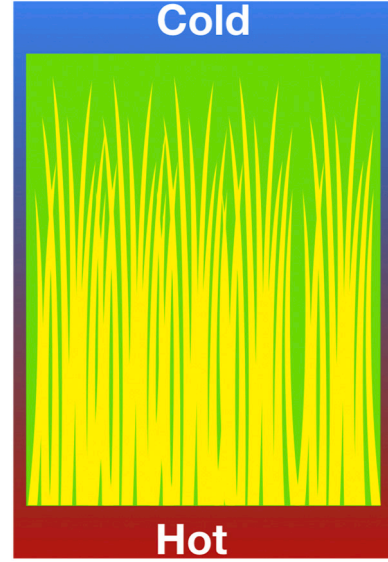

Fig. 3. The ambient phase (in green) is a porous deformable matrix in which the much less viscous fluid (in yellow), percolates. The mixture is submitted to a temperature gradient. (For interpretation of the references to colour in this figure legend, the reader is referred to the web version of this article.)
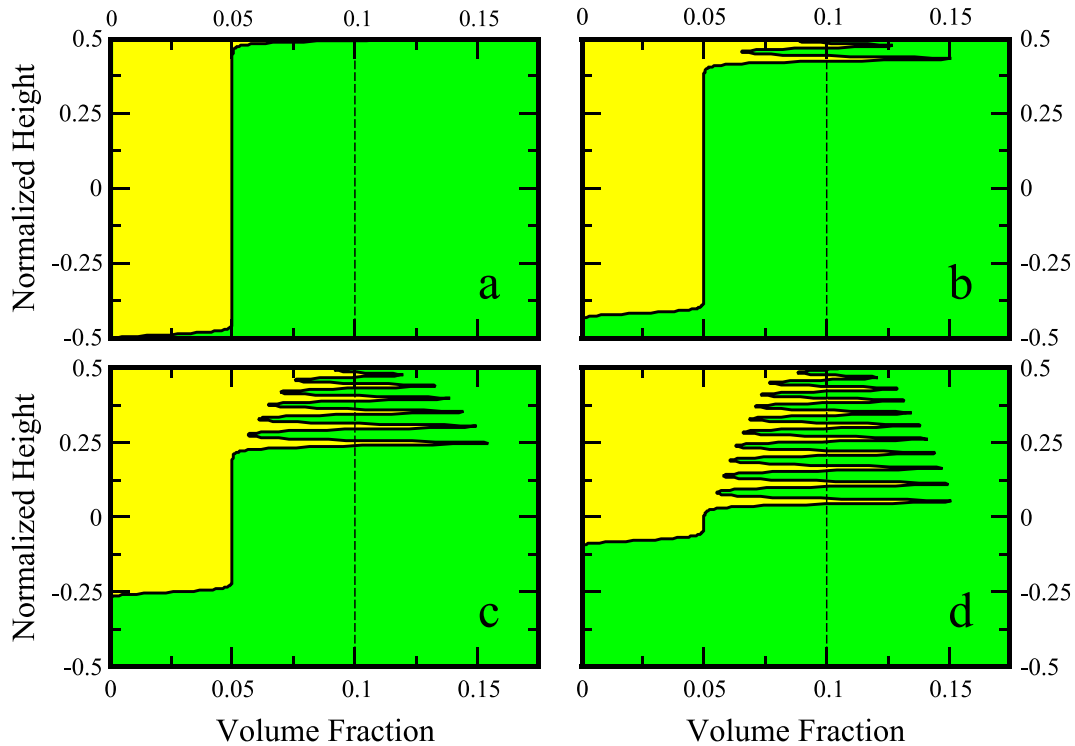

Fig. 2. Four snapshots at different times of the volume fraction of the bubbles. The horizontal axis is the volume fraction ϕ, the vertical axis is the height. The minor phase (in yellow) is less dense and much less viscous than the ambient phase (in green). Above the dashed line, $\phi = 0.1$, the Marangoni force is larger than buoyancy. The parameter values are those of an experiment by Young et al. (1959). The ambient fluid is n-hexadecane with density $\rho_o = 770$ kg m^{-3}, viscosity $\mu_o = 3.52 \times 10^{-3}$ Pa s and a surface tension of 27.66×10^{-3} N m^{-1} that we identify to $3\sigma_e$. The gas bubbles have a mean radius of $r = 10^{-4}$ m. The capillary length is $l_c = 3.7$ cm, the Stokes velocity of a single bubble $v_s = 7.1$ mm s^{-1}. In their experiment, Young et al. (1959) hold an isolated bubble stationary by imposing a vertical temperature gradient of -75 K cm^{-1} as for n-hexadecane, $d\sigma/dT = -0.1 \times 10^{-3}$ N m^{-1} K^{-1}. The height of the experiment is not given in their paper and we assume a height $h = 1$ cm $= 0.27$ l_c. The snapshots, a, b, c, and d, correspond to times of 0.8, 2.5, 7.4 and 12.6 s, respectively. (For interpretation of the references to colour in this figure legend, the reader is referred to the web version of this article.)

geophysical situations.

2.4.1. Case of a homogeneous solid

In this case, we consider a simple ambient matrix crossed by tubules of radius r, with 3 orthogonal tubules in each cube of side b made of a homogeneous deformable highly viscous phase (Turcotte and Morgan, 1992). Here we assume that b is a constant and only the section of the liquid tubules can change with the porosity.

In this case, the porosity and surface area are simply $\phi = 3\pi r^2/b^2$ and $\alpha = 6\pi r/b^2$ so that

$$\alpha = \frac{2\sqrt{3\pi}}{b}\sqrt{\phi}. \tag{29}$$

The interaction term c that controls the shear between the two phases is related to the permeability of the matrix $k = \phi r^2/24 = \phi^2 b^2/(72\pi)$ (Turcotte and Morgan, 1992) and to the viscosity of the fluid. We show in Bercovici et al. (2001) that $c = \mu_i \phi^2/k$ and c is therefore a constant in this model, $c = 72\pi\mu_i/b^2$.

The above tubule model only holds at small porosity. When the tubules are in contact, $r = b/2$, the system crosses a threshold of disaggregation, above which, instead of a liquid percolating through a solid, the mixture is comprised of a slurry of isolated solid grains surrounded by liquid (Hier-Majumder et al., 2006). In this case, the relative motion of phases is described by the model of Stokes flow discussed earlier, and $\alpha = 3(1 - \phi)/(b/2)$ as in eq. (21) (except that now, the travelling solid is in proportion $1 - \phi$ and made of drops of size $b/2$). It is clear that our model does not accurately describe the transition in flow when jumping from tubules of liquid to grains of solid, nor does it provide a representation of the interface area that occurs near the disaggregation limit; however, disaggregation is not central for this paper.

With this model, in the case of a Darcy flow, one has (using A for the geometrical factor $2\sqrt{3\pi}$)

$$\frac{d}{dz}\sigma_e\frac{\partial\alpha}{\partial\phi} = \frac{A}{b}\left(\frac{1}{2\sqrt{\phi}}\frac{d\sigma_e}{dz} - \frac{\sigma_e}{4\phi^{3/2}}\frac{d\phi}{dz}\right),$$
$$\frac{d\sigma_e\alpha}{dz} - \sigma_e\frac{\partial\alpha}{\partial\phi}\frac{d\phi}{dz} = \frac{A}{b}\sqrt{\phi}\frac{d\sigma_e}{dz}, \tag{30}$$

and the characteristic velocity of the liquid phase, $V_i = (1 - \phi)F/\phi$ (see (15)), is proportional to the forcing term F with

$$F = \frac{\phi^2}{72\pi\mu_i}\left[(1 - \phi)\Delta\rho g b^2 - Ab\frac{1 + \phi}{2\sqrt{\phi}}\frac{d\sigma_e}{dz} + Ab\sigma_e\frac{1 - \phi}{4\phi^{3/2}}\frac{d\phi}{dz}\right] \tag{31}$$

The driving term shows a major difference with the case of a foam behavior expressed in (25). This time there is a third term related to the gradient of porosity which always leads to phase separation (Ricard et al., 2001): it has the form $\xi\nabla\phi$ with $\xi > 0$, which introduced into the phase evolution eq. (9), leads to an anti-diffusive term $-\nabla.(\xi\nabla\phi)$. This is the expected self-separation behavior of surface tension in, for example, oil-water mixtures. This self-separation did not occur in our previous examples of Stokes drag in emulsions or foams, for which we have assumed that the bubble radii are fixed and therefore there was no decrease of surface energy (except in the Marangoni term) in separating the phases (see also Appendix A).

The Marangoni term (second term inside the square parenthesis) is also present and particularly active at small porosity. Like in the case of a Stokes flow, it drives the liquid in the direction of the thermal gradient, since A is positive and therefore against gravity when the top boundary is colder than the bottom one.

2.4.2. Case of a solid made of grains

In geological applications, the solid in which a liquid can percolate is typically made of grains. As the crystal lattice in each grain has a different orientation, the interface between grains has also a solid-solid surface tension which can be larger than the solid-liquid surface tension.

We must therefore consider both the surface energy of liquid-solid interfaces, increasing when the liquid wets the grain boundary and the surface energy of solid-solid interfaces decreasing by absorption of liquid. The two surface tensions are assumed to be only functions of temperature and their ratio is assumed constant.

As in Hier-Majumder et al. (2006), we express the surface energy as the sum of what is carried by the liquid-solid interfaces (with surface tension σ_{oi} and interface area density α_{oi}) and by the solid-solid interfaces (with surface tension σ_{oo} and interface area density α_{oo}).

$$\chi = \sigma_{oi}\alpha_{oi} + \sigma_{oo}\alpha_{oo} \tag{32}$$

For analytical simplicity we do not consider a solid made of complex 3D grains (Wimert and Hier-Majumder, 2012; Rudge, 2018) but made of 2D hexagonal columns where the liquid can percolate through the triple junction tubules. Following Hier-Majumder et al. (2006) and using θ for half the wetting (or semi-dihedral) angle (see Fig. 4), we obtain

$$\chi = \frac{\sigma_{oo}}{b}\left(\frac{\sigma_{oi}}{\sigma_{oo}}c_{oi}\sqrt{\phi} + \left(1 - c_{oo}\sqrt{\phi}\right)\right) = \sigma_{oo}b\left(1 + A\sqrt{\phi}\right) \tag{33}$$

with

$$c_{oi} = 2\frac{\sqrt{3}\psi}{\sqrt{2sin\psi cos(\theta/2) - \sqrt{3}\psi}},$$
$$c_{oo} = 2\frac{sin\psi}{\sqrt{2sin\psi cos(\theta/2) - \sqrt{3}\psi}}, \tag{34}$$
$$A = c_{oi}\frac{\sigma_{oi}}{\sigma_{oo}} - c_{oo}$$

where $\psi = \pi/6 - \theta/2$. These expressions are valid for $\theta \leq \pi/6$; for larger dihedral angles, the melt is trapped within disconnected bubbles (see von Bargen and Waff, 1986).

An equilibrium situation of the grain-grain and grain-liquid capillary forces at triple junctions is possible when the semi-dihedral angle can verify $\sigma_{oo}/\sigma_{oi} = 2\cos\theta$. This equilibrium exists from to $\theta = \pi/6$ (or $\sigma_{oo} = \sqrt{3}\sigma_{oi}$) to $\theta = 0$ (or $\sigma_{oo} = 2\sigma_{oi}$). High temperature experiments have
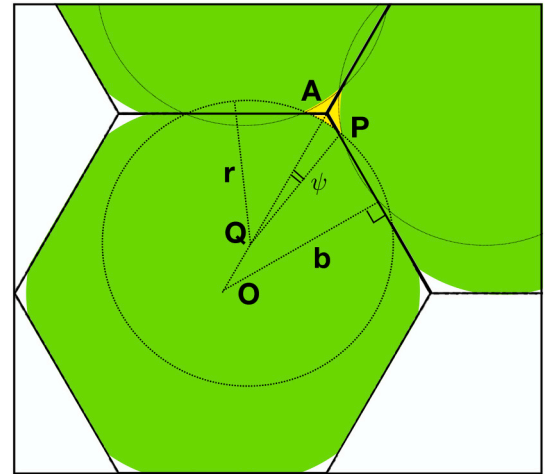

Fig. 4. A model of a mixture of fluid and grains is made of hexagonal columns (green) and the fluid resides in triple junctions, displayed in yellow around the point A. The tubules' cross-sections are limited by three portions of circles having a radius r and forming angles of 2θ at their intersections. In this figure, the center of one of the circles defining the tubule is in Q. The surface of a hexagon is $2b^2\sqrt{3}$, its center is at O and the angle $\widehat{AQP}$ is $\psi = \pi/6 - \theta/2$. The curvature r of the circle limiting the tubule is related to the porosity by $\phi = (r/b)^2(2sin\psi cos(\theta/2) - \psi\sqrt{3})$ (see details in Hier-Majumder et al. (2006)). (For interpretation of the references to colour in this figure legend, the reader is referred to the web version of this article.)

documented the infiltration of liquid metal into silicates (Knittle and Jeanloz, 1991; Goarant et al., 1992; Terasaki et al., 2008; Yoshino, 2019). These experiments indicate therefore that $\sigma_{oo}/\sigma_{oi} \geq \sqrt{3}$ at CMB conditions, but no precise measurement of this ratio is available and much larger values are possible. The equilibrium in this case, assuming that the only forces under consideration are uniform surface tensions, corresponds to complete grain wetting. However, metal penetration is subject to other forces such as gravity, Darcy friction or Marangoni force that may not allow this equilibrium. We therefore consider that $\sqrt{3} \leq \sigma_{oo}/\sigma_{oi} < +\infty$ and we use $\theta = 0$ when $\sigma_{oo} \geq 2\sigma_{oi}$. The term A in the third expression of (34) that appears in the total surface energy term, (33) is plotted in Fig. 5. It is negative in the whole range of wetting angles that allow percolation.

This model is valid until there is no solid-solid interfaces anymore, which occurs at the disaggregation limit $1 - c_{oo}\sqrt{\phi} = 0$ (see the first equality of eq. (33)); the minimum fluid fraction at the disaggregation limit is $\phi = 9.3\%$ when $\theta = 0$. As in our previous discussion with the homogeneous solid, a more complex micromechanical model would be needed to account for the transition from a connected matrix to a crystal slurry.

Again we express the different derivatives assuming that the semi-dihedral angle does not change with the temperature and we get

$$\frac{\mathrm{d}}{\mathrm{d}z}\frac{\partial\chi}{\partial\phi} = \frac{A}{b}\left(\frac{1}{2\sqrt{\phi}}\frac{\mathrm{d}\sigma_{oo}}{\mathrm{d}z} - \frac{\sigma_{oo}}{4\phi^{3/2}}\frac{\mathrm{d}\phi}{\mathrm{d}z}\right)$$

$$\frac{\mathrm{d}\chi}{\mathrm{d}z} - \frac{\partial\chi}{\partial\phi}\frac{\mathrm{d}\phi}{\mathrm{d}z} = \frac{1}{b}\left(1 + A\sqrt{\phi}\right)\frac{\mathrm{d}\sigma_{oo}}{\mathrm{d}z}$$

(35)

and the forcing term F

$$F = \frac{\phi^2}{cb^2}\left[(1-\phi)\Delta\rho gb^2 - b\left(1 + A\frac{1+\phi}{2\sqrt{\phi}}\right)\frac{\mathrm{d}\sigma_{oo}}{\mathrm{d}z} + Ab\sigma_{oo}\frac{1-\phi}{4\phi^{3/2}}\frac{\mathrm{d}\phi}{\mathrm{d}z}\right]$$

(36)

This equation is similar to (31) except that A is now negative instead of positive and therefore, the Marangoni term ($|A|/\sqrt{\phi}\gg 1$ at small porosity) and the term proportional to the gradient of ϕ have both changed signs. As $\mathrm{d}\sigma_{oi}/\mathrm{d}T < 0$, the Marangoni term drives now the minor
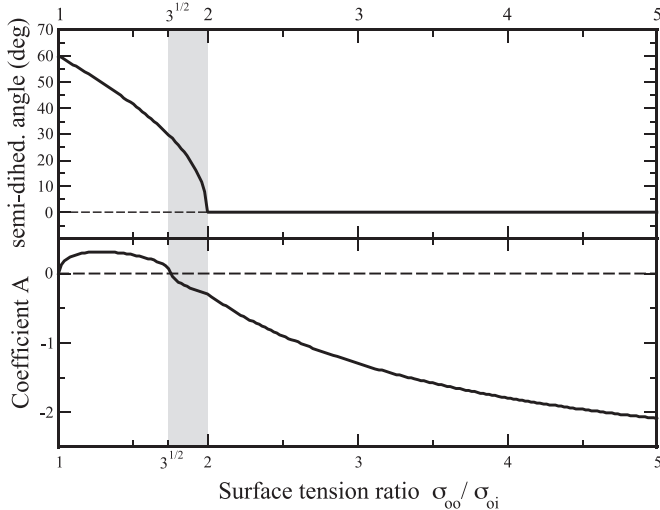

Fig. 5. Semi-dihedral angle θ (top) and parameter A (bottom) of our mixture model as a function of the surface tension ratio σ_{oo}/σ_{oi}. At small liquid fraction, percolation is only possible when $\sigma_{oo}/\sigma_{oi} \geq \sqrt{3}$, in which case A is negative and reaches asymptotically the value $c_{oo} = -3.27$ when $\sigma_{oo} \gg \sigma_{oi}$ (see (34)). On the left of the zone in grey $\sigma_{oo}/\sigma_{oi} \leq \sqrt{3}$, the semi-dihedral angle is larger than 30° and a minimum value of the fluid volume fraction must be exceeded before a network of connected pores can exist. In the grey zone a stable network of tubules is possible. On the right of the zone in grey $\sigma_{oo}/\sigma_{oi} \geq 2$, the liquid phase tends to totally wet the grains.

phase (metal) toward the cold boundary, in the direction opposite to the temperature gradient. If we consider the situation where liquid metal percolates through the matrix, $\Delta\rho$ is negative but the Marangoni force tends to soak metal from the core into the overlying colder silicates. The term associated with the gradient of porosity appears like a diffusive term in transport eq. (9) and tends to homogenize the liquid phase into the matrix and therefore to favor the infiltration of the metal into the silicates (Poirier and Le Mouël, 1992; King et al., 2011; Hier-Majumder et al., 2006).

We have not discussed the Darcy drag factor c in detail for this case of polygonal grains. This factor can be expressed as $\mu_i\phi^2/k$ (see section 2.4.1) where the permeability k is controlled by ϕ times the typical cross-sectional area of the liquid tubules. The shape of a tubule, at the intersection of three cylinders, does not permit a simple analytical solution but the equivalent cross-section of the tubule is a fraction of ϕb^2 and therefore c should be a constant. The Darcy flow experiences less drag when ϕ is large as the radius of a pore is not b but rather a fraction of $b\sqrt{\phi}$.

3. Orders of magnitude and general comments

The force balance relation is given by (13) with F given by (36); we then normalize the velocities by a Darcy velocity $|\Delta\rho| g/c$, surface tension σ_{oo} by a reference σ_0, the height z by the capillary length $l_c = \sigma_0/(|\Delta\rho|gb)$ and introduce the compaction length $\delta^2 = 4\mu_o/(3cl_c^2)$ (assuming c constant), in which case, (13) becomes

$$\delta^2\phi^2\frac{\mathrm{d}}{\mathrm{d}\widetilde{z}}\left(\frac{1-\phi^2}{\phi}\frac{\mathrm{d}\widetilde{v}_o}{\mathrm{d}\widetilde{z}}\right) - \widetilde{v}_o = F,$$

(37)

with

$$F = \phi^2\left[\epsilon(1-\phi) + A\widetilde{\sigma}\frac{1-\phi}{4\phi^{3/2}}\frac{\mathrm{d}\phi}{\mathrm{d}\widetilde{z}} - \left(1 + A\frac{1+\phi}{2\sqrt{\phi}}\right)\frac{\mathrm{d}\widetilde{\sigma}}{\mathrm{d}\widetilde{z}}\right],$$

(38)

the variables with a tilde have no dimensions and ϵ is -1 for a dense liquid metal in a silicate matrix.

In the next subsections, we summarize the implications of (37) and (38) in the context of metal-silicate separation in laboratory experiments, at the core-mantle boundary and in planetesimals. In these three situations, the relevant model entails Darcy flow of a dense liquid phase (metal) within a silicate matrix but the ratios of capillary forces and gravity are very different.

3.1. Laboratory conditions

We first consider laboratory conditions at uniform temperature and an experiment of metal-silicate separation in a millimetric volume containing a mixture of metallic alloy and silicates with a typical grain size of $b = 10$ μm. The metallic alloy used in Terasaki et al. (2012), has the eutectic composition $Fe_{60}S_{40}$ and a density of 4500 kg m^{-3} (we use $\Delta\rho = 1200$ kg m^{-3}). The capillary length is $l_c = 8.33$ m and the experiments are performed in a cell of height $h = 3$ mm (from $z = -h/2$ to $z = h/2$). As the liquid-solid surface tension of the metallic alloy decreases with the sulphur content, we assume perfect wetting and take $\theta = 0$. According to the eq. (34), A is a negative number between -3.27 and -0.6 (see Fig. 5) and we choose $A = -2$ for numerical applications. In the absence of the Marangoni force, and assuming an experiment of infinite size, the equilibrium between gravity and surface tension in (38), implies that

$$-(1-\phi) + A\widetilde{\sigma}\frac{1-\phi}{4\phi^{3/2}}\frac{\mathrm{d}\phi}{\mathrm{d}\widetilde{z}} = 0,$$

(39)

in which case the porosity obeys

$$\phi = \frac{\phi_0}{(1 + z/H)^2} \tag{40}$$

with $H = |A|l_c/\left(2\sqrt{\phi_0}\right)$ and where ϕ_0 is the metal content at $z = 0$ (experimentally, the total metal proportion in the cell, ϕ_m is imposed and $\phi_0 = \phi_m/(1 + \phi_m h^2/|A|^2 l_c^2)$). In metal-silicate separation experiments performed at uniform temperature, i.e., in the absence of Marangoni forces, the capillary length is much larger than the sample size ($h/l_c = 3.6 \times 10^{-4}$ with the chosen parameters) and the dominant force is the surface tension which homogenizes the metal content. According to (40), in a metal-silicate laboratory experiment performed with a $h = 3$ mm high sample containing 50% of liquid metal, the dense metal content would only decrease with height from 50.02% to 49.98%.

We consider now a laboratory experiments done in the presence of a temperature gradient according to the conditions described in Labrosse et al. (2010). The set-up of these experiments is purposely chosen to allow large temperature gradients and minimize the chemical reactions between phases (contrary to the situations described in Yoshino (2019)). The temperature drops linearly with z, $T = \overline{T} - (z/h)\Delta T$ (with $\Delta T = 350$ K, $h = 3$ mm, and $\overline{T} = 1750$ K). The metal-silicate surface tension decreases exponentially with temperature as $\sigma_0 exp\left(-\left(T - \overline{T}\right)/T_0\right)$ with $T_0 \approx 1400$ K. The normalized gradient of surface tension varies therefore like

$$\frac{d\widetilde{\sigma}}{d\widetilde{z}} = \frac{\Delta T}{T_0} \frac{1}{\widetilde{h}} \exp\left(\frac{\widetilde{z}}{\widetilde{h}} \frac{\Delta T}{T_0}\right) \tag{41}$$

Having shown gravity to be negligible, the equilibrium between the Marangoni and homogeneous surface tension forces in (38),implies

$$A\widetilde{\sigma}\frac{1 - \phi}{4\phi^{3/2}} \frac{d\phi}{d\widetilde{z}} - \left(1 + A\frac{1 + \phi}{2\sqrt{\phi}}\right) \frac{d\widetilde{\sigma}}{d\widetilde{z}} = 0 \tag{42}$$

which yields, assuming $\phi \ll 1$ and with $\Delta T \ll 2T_0$,

$$\phi \approx \phi_0 exp\left(2\frac{\Delta T}{T_0} \frac{z}{h}\right) \tag{43}$$

This result implies that the dense metal will move toward the cold side of the experiment, irrespectively of gravity. With the chosen numerical factors, the metal volume fraction will go from ϕ_0 at the hot side to 1.65 ϕ_0 near the cold side. Therefore, the Marangoni force will control the metal migration and final distribution.

This is confirmed by the full numerical simulation (see Fig. 6) where the eqs. (37)–(38) are solved using a tridiagonal solver with zero velocities on the top and bottom boundaries and the advection (9) by an explicit upwind scheme. To reach the equilibrium in a time comparable to that necessary in a laboratory experiment (a few mm in a day), we choose $c = 3.0 \times 10^{13}$ Pa s m^{-2}. As c is related to the fluid phase viscosity divided by the tubule cross-sections (see e.g., Bercovici et al., 2001) μ_i would be of order 30 Pa s for tubules of diameters 1 μm. We take $\delta = 0.01$ which implies a viscosity μ_o for the solid phase of only a X 1.56 X 10^9 Pa s. The high temperature of the experiment with the presence of liquid alloy and a silicate probably not far from its own melting temperature withouts this low value. The choice of these parameters is largely arbitrary but the compaction length, and therefore the matrix viscosity, cannot be too large otherwise the phase separation becomes very slow. The numerical simulation depicted in Fig. 6 leads to a moderate variation of the metal fraction with height. As the surface tension appears in both the Marangoni force and in the term that tends to homogenize the metal content, the final equilibrium does not depend on its absolute value. The dependence of the equilibrium depends only weakly on the
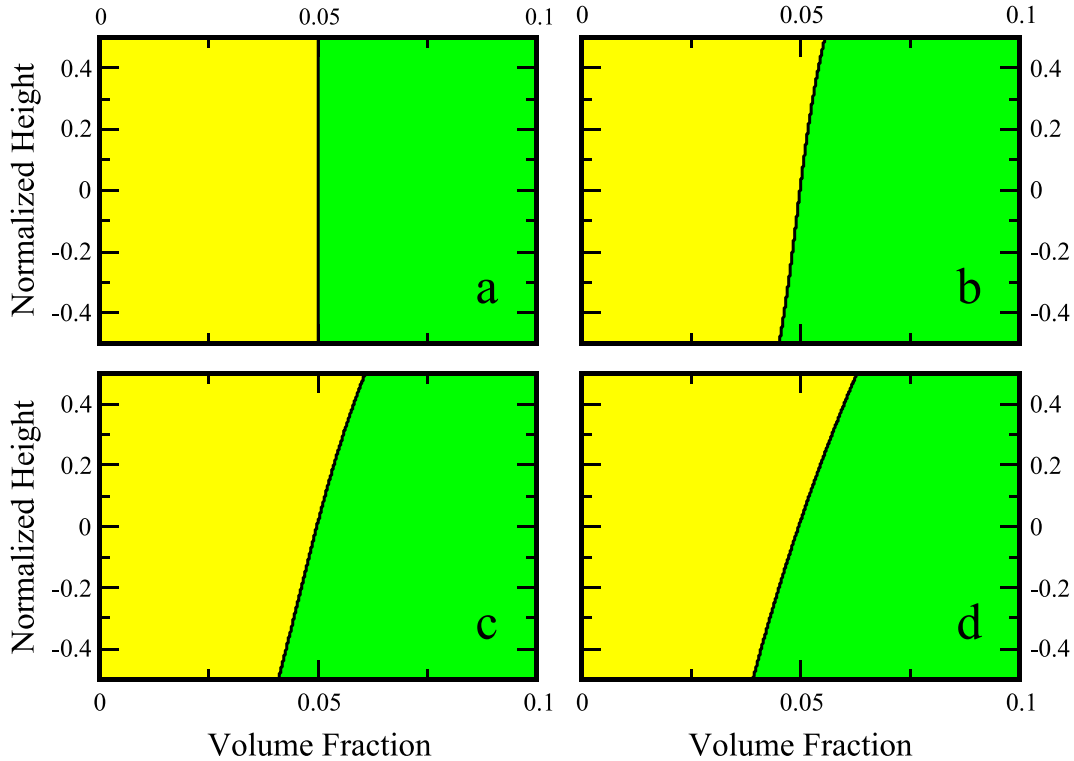

Fig. 6. Four snapshots at different times of the volume fraction of the phases. The horizontal axis is the metal volume fraction ϕ, the vertical axis is the height. The initial metal volume fraction is 0.05. The gravity is negligible compared to the surface tension forces and cannot separate the dense metal phase from the silicates. The surface tension tends to homogenize the metal fraction while the Marangoni force pushes the metal in the direction of the upper colder boundary. The snapshots of Fig. 6, a, b, c, and d are taken at times 0.6 h, 1.44 h, 4.42 h and 24 h, respectively. The panel d is very close to the final equilibrium ($c = 3.0 \times 10^{13}$ Pa s m^{-1}, $\mu_0 = $ a X 1.56 X 10^9 Pa s, $A = -2$, $\Delta\rho = 1200$ kg m^{-3}).

negative value of A which does not appear in the approximate eq. (43).

3.2. CMB conditions

If we wish to apply our model to the core-mantle boundary with $\Delta\rho = 3500 \text{ kg m}^{-3}$, we must consider grain sizes around 1 mm implying $b = 0.5$ mm, in which case the capillary length is 5.7 cm and we choose $A = -2$. In the case of a homogeneous surface tension, the equilibrium between gravity and surface tension given by (39) implies a metal content still given by (40) where z is now the unbounded height above the CMB and $\phi_0 = 1$ is the metal content at the contact with the core. In our model, the capillary forces increase with decreasing tubule cross-sectional area, which is proportional to ϕ (Fig. 4); since ϕ decreases with z, the capillary forces only get stronger with height, which explains why the elevation at which the metal can rise is effectively unbounded (although the metal volume fraction becomes vanishingly small for $z \gg |A| l_c/2$). The metal would only be lifted by a few meters as the metal content would decrease from 100% to 0.01% in 5.7 m) in keeping with previous findings (see e.g., Poirier and Le Mouël, 1992).

According to (37), the balance between the Marangoni force and gravity occurs when

$$(1-\phi) + \left(1 + A\frac{1+\phi}{2\sqrt{\phi}}\right)\frac{d\widetilde{\sigma}}{d\widetilde{z}} = 0. \tag{44}$$

This relation indicates that the Marangoni suction is larger when the metal melt fraction is small. It becomes comparable to gravity when the negative thermal gradient is

$$\left|\frac{dT}{dz}\right| = \frac{2\sqrt{\phi}}{|A|}\frac{T_0}{l_c}. \tag{45}$$

Even considering a very small metal content, $\phi = 10^{-6}$, eq. (45) corresponds to a thermal gradient of 1000 K over a few meters that does not seem plausible and hence the Marangoni force is negligible at CMB conditions. If metal is trapped in the deep mantle above the CMB, it is likely due to other processes such as sedimentation from the core side (Buffett et al., 2000) or infiltration due to the fact that the core-mantle boundary is not an equipotential (Kanda and Stevenson, 2006).

3.3. Asteroid conditions

We next consider the application of our model to metal-silicate segregation in asteroids. Asteroid densities are usually very low, around 1.5 kg m^{-3} (Carry, 2012) as their porosity is large and their gravitational force too weak to induce compaction. For a planetesimal of radius 10 km (assuming such a small body has a spherical form), the gravity should be only of order 4×10^{-4} that of the Earth which, for

similar 1 mm grains, would increase the capillary length to 142 m. According to (40), surface tension would be able to hold a liquid metal against gravity, with 0.02% of liquid metal at the surface and pure metal at the planetesimal center (assuming liquid metal can reside at the surface without crystallizing).

To estimate the importance of Marangoni forces in small asteroids, one can consider an internally molten asteroid of radius R with a cold near surface layer of thickness $d = R/10$. The temperature difference across this layer, between liquid silicates and the outer space is comparable to the melting temperature of silicates which is of order T_0. In the bottom part of this lithosphere, the temperature allows the metal to be liquid while the silicates remain solid. According to (45), the Marangoni suction was larger than gravity when the metal melt fraction was small and until its fraction was 2%. Such a liquid metal fraction is rather low, implying that the Marangoni force does not play a major role in planetesimal differentiation; although asteroidal gravities are very small compared of that on Earth, their potential thermal gradients are likely much smaller than what occurs in laboratory experiments. Nevertheless, the metal content (2%) below which the Marangoni forces should suck the metal to the surface suggests that the Marangoni effect might drive melt ejection from the most compacted mush, inside the planetesimal, toward a shallow freezing front, and therefore deposit a significant metal fraction at the surface. This effect might help explain the presence of a significant metal percentage at the surface of M-type asteroids (Shepard et al., 2015) including Psyche (Elkins-Tanton et al., 2020).

The complete discussion of the role of surface forces in the phase segregation inside planetesimals remains to be done particularly to quantify the interactions between the time-scales of their size evolution, of their temperature evolution, and of the metal transport. The very low gravity of these body makes the importance of the capillary forces not entirely negligible with respect to compositional buoyancy in the zone beneath their cold boundary layer where the thermal gradients are large and the metal liquid. A realistic model of growing and convecting planetesimals undergoing differentiation is however beyond the goal of this paper.

Declaration of Competing Interest

The authors declare that they have no known competing financial interests or personal relationships that could have appeared to influence the work reported in this paper.

Acknowledgment

Appendix A. Constant number density of bubbles

The linear or non-linear relation between the density of interfacial area, α and the volume fraction of the minor phase, controls whether the mixture ultimately undergoes a self-separation of the two phases. In the model of a foamy medium where the number density and the volume fraction of bubbles are independent variables, then, $\alpha = 3\phi/r = 3^{2/3}(4\pi\mathscr{N})^{1/3}\phi^{2/3} = \alpha_0\phi^{2/3}$, i.e., α is a non-linear function of ϕ. In this case, the interface curvature is $\partial\alpha/\partial\phi = 2/r$ as expected for spheres, and one has

$$\frac{d}{dz}\widetilde{\sigma}\frac{\partial\alpha}{\partial\phi} = \frac{2}{3}\alpha_0\phi^{-1/3}\frac{d\widetilde{\sigma}}{dz} - \frac{2}{9}\alpha_0\widetilde{\sigma}\phi^{-4/3}\frac{d\phi}{dz} = \frac{2}{r}\frac{d\widetilde{\sigma}}{dz} - \frac{2}{3r\phi}\widetilde{\sigma}\frac{d\phi}{dz},$$

$$\frac{d\widetilde{\sigma}\alpha}{dz} - \widetilde{\sigma}\frac{\partial\alpha}{\partial\phi}\frac{d\phi}{dz} = \alpha_0\phi^{2/3}\frac{d\widetilde{\sigma}}{dz} = \frac{3}{r}\phi\frac{d\widetilde{\sigma}}{dz}. \tag{46}$$

This leads (with $\omega = 0$) to

$$V_i = \frac{(1-\phi)^{p+1}}{3\mu_o}\left[(1-\phi)\Delta\rho g r^2 - (2+\phi)r\frac{d\widetilde{\sigma}}{dz} + \frac{2}{3}\frac{(1-\phi)}{\phi}r\widetilde{\sigma}\frac{d\phi}{dz}\right] \tag{47}$$

In this case, the Marangoni term is still present although slightly reduced (compare with (27)) and a new term appears, related to $d\phi/dz$. This term

will force the self-separation of the two phases, as in all cases where the dependence of α with ϕ is non-linear.

Credit authorship contribution statement

Y. Ricard: Conceptualization, Methodology, Software, Formal analysis, Writing - original draft. Stéphane Labrosse: Conceptualization, Formal analysis, Writing - review & editing. H. Terasaki: Investigation, Writing - review & editing. David Bercovici: Formal analysis, Writing - review & editing.

References

Batchelor, G.K., 1972. Sedimentation in a dilute dispersion of spheres. J. Fluid Mech. 52, 245.

Batchelor, G.K., 2000. *An Introduction to Fluid Dynamics*. Cambridge Mathematical Library. Cambridge University Press.

Bénard, H. (1900). Les tourbillons cellulaires dans une nappe liquide. *Revue générale des Sciences pures et appliquées, 11, 1261–1271 and 1309–1328.*

Bénard, H., 1901. Les tourbillons cellulaires dans une nappe liquide transportant de la chaleur par convection en régime permanent. Annales de Chimie et de Physique 23, 62–144.

Bercovici, D. (2007). Mantle dynamics, past, present and future: An overview,. In New-York, editor, *Treatise on Geophysics, 2ed,* vol. 7*, Mantle Dynamics, D. Bercovici editor; G. Schubert, editor in chief,* pages 1–22. Elsevier.

Bercovici, D., Michaut, C., 2010. Two-phase dynamics of volcanic eruptions: compaction, compression and the conditions for choking. Geophys. J. Int. 182 (2), 843–864.

Bercovici, D., Ricard, Y., 2003. Energetics of a two-phase model of lithospheric damage, shear localization and plate-boundary formation. Geophys. J. Int. 152 (3), 581–596.

Bercovici, D., Ricard, Y., 2005. Tectonic plate generation and two-phase damage: Void growth versus grain size reduction. J. Geophys. Res. 110 (B3).

Bercovici, D., Ricard, Y., 2012. Mechanisms for the generation of plate tectonics by two-phase grain-damage and pinning. Phys. Earth Planet. Inter. 202, 27–55.

Bercovici, D., Ricard, Y., 2014. Plate tectonics, damage and inheritance. Nature 508 (7497), 513.

Bercovici, D., Ricard, Y., Schubert, G., 2001. A two-phase model for compaction and damage 1. General Theory. J. Geophys. Res. 106 (B5), 8887–8906.

Block, M.J., 1956. Surface Tension as the Cause of Bénard Cells and Surface Deformation in a Liquid Film. Nature 178 (4534), 650–651.

Buffett, B., Garnero, E., Jeanloz, R., 2000. Sediments at the top of Earth's core. Science 290 (5495), 1338–1342.

Carry, B., 2012. Density of asteroids. Planetary Space Sci. 73 (1), 98–118.

Clift, R., Grace, J.R., Weber, M.E., 1978. Bubbles, Drops, and Particles. New York, dover pub inc edition, Mineola.

Drew, D.A., Segel, L.A., 1971. Averaged equations for 2-phase flows. Studies In Appl. Mathematics 50, 205–220.

Elkins-Tanton, L.T., Asphaug, E., Bell III, J.F., Bercovici, H., Bills, B., Binzel, R., Bottke, W.F., Dibb, S., Lawrence, D.J., Marchi, S., McCoy, T.J., Oran, R., Park, R.S., Peplowski, P.N., Polanskey, C.A., Prettyman, T.H., Russell, C.T., Schaefer, L., Weiss, B.P., Wieczorek, M.A., Williams, D.A., Zuber, M.T., 2020. Observations, meteorites, and models: A preflight assessment of the composition and formation of (16) psyche. J. Geophys. Res. 125 (3).

Faroughi, S.A., Huber, C., 2015. Unifying the relative hindered velocity in suspensions and emulsions of nondeformable particles. Geophys. Res. Lett. 42 (1), 53–59.

Goarant, F., Guyot, F., Peyronneau, J., Poirier, J., 1992. High-pressure and high-temperature reactions between silicates and liquid-iron alloys, in the diamond anvil cell, studied by analytical electron-microscopy. J. Geophys. Res. 97 (B4), 4477–4487.

Haberman, W., Morton, R., 1953. An experimental investigation of the drag and shape of air bubbles rising in various liquids. Technical report, Report. Navy Department, The David W. Taylor Model Basin, p. 802.

Hardy, S., 1979. Motion Of Bubbles In A Vertical Temperature-Gradient. J. Colloid Interface Sci. 69 (1), 157–162.

Harper, J., Moore, D., Pearson, J., 1967. Effect of variation of surface tension with temperature on motion of bubbles and drops. J. Fluid Mech. 27 (2), 361.

Hier-Majumder, S., Kohlstedt, D., 2006. Role of dynamic grain boundary wetting in fluid circulation beneath volcanic arcs. Geophys. Res. Lett. 33 (8).

Hier-Majumder, S., Ricard, Y., Bercovici, D., 2006. Role of grain boundaries in magma migration and storage. Earth Planet. Sci. Lett. 248, 735–749.

Kanda, R., Stevenson, D., 2006. Suction mechanism for iron entrainment into the lower mantle. Geophys. Res. Lett. 33 (2).

King, D.S.H., Hier-Majumder, S., Kohlstedt, D.L., 2011. An experimental study of the effects of surface tension in homogenizing perturbations in melt fraction. Earth Planet. Sci. Lett. 307 (3–4), 349–360.

Knittle, E., Jeanloz, R., 1991. Earths core-mantle boundary - results of experiments at high-pressures and temperatures. Science 251 (5000), 1438–1443.

Labrosse, S., Terasaki, H., Ricard, Y., 2010. Marangoni effect in metal-silicate self separation, Vol 12. EGU2010-4513, Vienna, Autria.

Marangoni, C., 1871. Ueber die ausbreitung der tropfen einer flüssigkeit auf der oberfläche einer anderen. Ann. Phys. 219 (7), 337–354.

McKenzie, D., 1984. The generation and compaction of partially molten rock. J. Petrol. 25, 713–765.

Michaut, C., Ricard, Y., Bercovici, D., Sparks, R.S.J., 2013. Eruption cyclicity at silicic volcanoes potentially caused by magmatic gas waves. Nat. Geosci. 6 (10), 856–860.

Poirier, J., Le Mouël, J., 1992. Does infiltration of core material into the lower mantle affect the observed geomagnetic-field. Phys. Earth Planet. Inter. 73 (1-2), 29–37.

Rabinowicz, M., Ricard, Y., Gregoire, M., 2002. Compaction in a mantle with a very small melt concentration: Implications for the generation of carbonatitic and carbonate-bearing high alkaline mafic melt impregnations. Earth Planet. Sci. Lett. 203, 205–220.

Rasmussen, K., Haack, H., Ulff-Moller, F., 2001. Metallographic cooling rates of group IIF iron meteorites. Meteorit. Planet. Sci. 36 (7), 883–896.

Ricard, Y., Bercovici, D., 2009. A continuum theory of grain size evolution and damage. J. Geophys. Res. 114.

Ricard, Y., Bercovici, D., Schubert, G., 2001. A two-phase model for compaction and damage 2. Applications to compaction, deformation, and the role of interfacial surface tension. J. Geophys. Res. 106, 8907–8924.

Ricard, Y., Bercovici, D., Albarede, F., 2017. Thermal evolution of planetesimals during accretion. Icarus 285, 103–117.

Richardson, J.F., Zaki, W.N., 1954. The sedimentation of a suspension of uniform spheres under conditions of viscous flow. Chem. Eng. Sci. 3 (2), 65–73.

Rudge, J.F., 2018. Textural equilibrium melt geometries around tetrakaidecahedral grains. Proc. Royal So. 474 (2212).

Scott, D.R., Stevenson, D.J., 1984. Magma solitons. Geophys. Res. Lett. 11, 9283–9296.

Shepard, M.K., Taylor, P.A., Nolan, M.C., Howell, E.S., Springmann, A., Giorgini, J.D., Warner, B.D., Harris, A.W., Stephens, R., Merline, W.J., Rivkin, A., Benner, L.A.M., Coley, D., Clark, B.E., Ockert-Bell, M., Magri, C., 2015. A radar survey of M- and X-class asteroids. III. Insights into their composition, hydration state, & structure. Icarus 245, 38–55.

Spiegelman, M., 1993. Flow in deformable porous-media. 2. numerical-analysis - the relationship between shock-waves and solitary waves. J. Fluid Mech. 247, 39–63.

Šrámek, O., Milelli, L., Ricard, Y., Labrosse, S., 2012. Thermal evolution and differentiation of planetesimals and planetary embryos. Icarus 217 (1), 339–354.

Terasaki, H., Frost, D.J., Rubie, D.C., Langenhorst, F., 2008. Percolative core formation in planetesimals. Earth Planet. Sci. Lett. 273 (1–2), 132–137.

Terasaki, H., Urakawa, S., Rubie, D.C., Funakoshi, K.-i., Sakamaki, T., Shibazaki, Y., Ozawa, S., Ohtani, E., 2012. Interfacial tension of Fe-Si liquid at high pressure: Implications for liquid Fe-alloy droplet size in magma oceans. Phys. Earth Planet. Inter. 202, 1–6.

Turcotte, D., Morgan, J.P., 1992. The physics of magma migration and mantle flow beneath a mid-ocean ridge. In: Morgan, J.P., Blackman, D., Sinton, J. (Eds.), Mantle Flow and Melt-Generation at Mid-Ocean Ridges, Geophys. Monogr. Ser., 71 Am. Geophys. Union, Washington, DC, pp. 155–182.

von Bargen, N., Waff, H., 1986. permeabilities, interfacial-areas and curvatures of partially molten systems - results of numerical computation of equilibrium microstructures. J. Geophys. Res. 91 (B9), 9261–9276.

Walter, M.J., Tronnes, R.G., 2004. Early Earth differentiation. Earth Planet. Sci. Lett. 225 (3–4), 253–269.

Wimert, J., Hier-Majumder, S., 2012. A three-dimensional microgeodynamic model of melt geometry in the Earth's deep interior. J. Geophys. Res. 117.

Yoshino, T., 2019. Penetration of molten iron alloy into the lower mantle phase. C. R. Acad. Sci. 351 (2–3), 171–181.

Yoshino, T., Walter, M.J., Katsura, T., 2003. Core formation in planetesimals triggered by permeable flow. Nature 422, 154–157.

Young, N., Goldstein, J., Block, M., 1959. The motion of bubbles in a vertical temperature gradient. J. Fluid Mech. 6 (3), 350–356.